Charged *soc* Metal-Organic Framework for High-Efficacy H_2 Adsorption and Syngas Purification: Atomistic Simulation Study

Jianwen Jiang
Dept. of Chemical and Biomolecular Engineering, National University of Singapore, Singapore 117576

DOI 10.1002/aic.11865
Published online July 16, 2009 in Wiley InterScience (www.interscience.wiley.com).

H_2 adsorption and syngas purification in charged soc *metal-organic framework are investigated using atomistic simulations. As experimentally observed, the extraframework NO_3^- ions are entrapped in carcerand-like capsule with negligible mobility. At low pressure, H_2 adsorption occurs concurrently at multiple sites near the exposed indium atoms and organic components. The capsule is accessible at high pressure through the surrounding channels by restricted windows. Adsorption sites identified are remarkably consistent with inelastic neutron scattering measurements. The isotherm and isosteric heat of H_2 adsorption predicted match well with experimental data. As loading rises, the isosteric heat remains nearly constant, revealing the homogeneity of adsorption sites. CO_2/H_2 selectivity in syngas adsorption is up to 600 and substantially higher than other nanoporous materials. With a trace of H_2O, the selectivity increases slightly at low pressure due to promoted adsorption of CO_2 by H_2O bound proximally to the exposed indium atoms, but decreases at high pressure as a consequence of competitive adsorption of H_2O over CO_2.* © 2009 American Institute of Chemical Engineers *AIChE J,* 55: 2422–2432, 2009

Keywords: H_2 adsorption, syngas purification, charged metal-organic framework, extraframework ions, atomistic simulations

Introduction

H_2 is considered as an ideal energy carrier and clean fuel for the future. A key issue for the practical utilization of H_2, for example, in mobile applications, is the development of safe and high-capacity systems for H_2 storage. The U.S. Department of Energy has set the targets for on-board H_2 storage as of 6.0 wt % and 45 g/L by 2010 and 9.0 wt % and 81 g/L by 2015.[1] For effective use of H_2, an equally important issue is to purify H_2 from syngas that is converted from a wide range of carbon materials, such as petroleum and coal. Currently, more than 95% of industrially used H_2 is produced through two reactions, steam-methane reformation $H_2O + CH_4 \rightarrow 3H_2 + CO$ and subsequently water-gas shift $H_2O + CO \rightarrow H_2 + CO_2$. The effluent gas (syngas) typically consists of 71–75% H_2, 15–20% CO_2, 4–7% CH_4, 1–4% CO, and trace of other gases such as H_2O.[2] To produce high-purity H_2 from syngas, H_2 needs to be separated from these gases.

Nanoporous materials such as zeolites and activated carbons have been proposed for H_2 storage and syngas separation.[3] Recently, metal-organic frameworks (MOFs) have emerged as an important class of hybrid inorganic–organic materials.[4] Composed of metal-oxide clusters and organic linkers, MOFs possess extremely large porosities ever recorded for crystalline materials and are highly regarded as promising candidates for gas storage, separation, and other important practical applications. Although a vast variety of nanoporous materials with different pore shapes and

Additional Supporting Information may be found in the online version of this article.

Correspondence concerning this article should be addressed to J. Jiang at chejj@nus.edu.sg

© 2009 American Institute of Chemical Engineers

dimensions have been synthesized, experimentally screening of a suitable material can be difficult and time-consuming. As an alternative, numerous simulation studies have been performed for H_2 storage and syngas purification. Simulations at atomic or molecular scale complement experiments provide fundamental insight and subsequently assist the rational design of novel materials and products. For example, a systematic simulation study was reported for H_2 in 12 purely siliceous zeolites, in which the cell parameters and framework flexibility were allowed to vary upon progressive filling of gas molecules.[5] Adsorption and diffusion of various gases including H_2 were investigated in all-silica zeolite MFI, AFI, FAU, CHA, DDR, and LTA; the correlation effects were found to depend on zeolite structure, pore size, and connectivity.[6] H_2 adsorption was reported in singe- and multiwalled carbon nanotubes, and the uptake in nanotube internal space was predicted to be lower than in the optimal graphitic nanofiber with slit-like pores.[7] The high-energy binding site for H_2 in IRMOF-1 was identified by simulation at the corner that quickly saturated with 1.27 H_2 molecules at 78 K, whereas a broad range of binding sites were observed at 300 K.[8] A simulation study of H_2 in 10 noncatenated MOFs revealed that H_2 uptake correlates well with isosteric heat at low pressure, with surface area and free volume separately at intermediate and high pressure.[9] The effect of catenation on interaction between H_2 and IRMOFs was simulated, and catenated frameworks were found to store H_2 more densely and exhibit a higher adsorption capacity than noncatenated counterparts.[10] Simulation of H_2 in three examples of IRMOF series demonstrated that catenation can be beneficial for improving H_2 storage at cryogenic temperatures and low pressure but not necessarily at room temperature.[11]

For syngas purification, CO_2/H_2 mixture in a microporous silica was simulated, and the selectivity of CO_2 over H_2 was compared with experimental data.[12] The separation of CO_2/H_2 mixtures was studied in silicalite and ETS-10 (Engelhard TitanoSilicate No. 10) and a larger selectivity was reported in ETS-10 at high pressure.[13] Activated carbons represented by a slit pore model were investigated for the separation of CO_2/H_2 mixture at different temperatures and pore sizes. The selectivity decreases monotonically as the pore size increases and reaches up to 90 at room temperature.[14] Adsorption of equimolar binary mixture of H_2 with CO_2 or CH_4 was simulated in a nanofiber with herringbone structure.[15] In dehydrated zeolite Na-4A, the simulated adsorption selectivity of CO_2/H_2 and CO_2/N_2 mixtures decreases slightly with increasing pressure at room temperature.[16] Simulation of syngas in IRMOF-1 and Cu-BTC showed that geometry, pore size, and electrostatic interaction affect separation efficiency for gas mixtures with components of different chemistries.[17]

In the ongoing quest for advanced porous materials, a unique subset of ion-exchanged MOFs have been recently developed. The presence of extraframework ions enhances the binding energy of adsorbate and hence affects adsorption and separation significantly. For example, various structural factors that might influence CO_2 adsorption on natural and synthetic zeolites were reported, in which the exchangeable ions were considered to play a key role.[18] Recently, Liu et al. synthesized a novel charged (square-octahedral) *soc*-MOF and found that H_2 adsorption in (dehydrated) *soc*-MOF reaches up to 2.61% at 78 K and 1.2 atm. Such a high capacity of H_2 has been rarely reported in MOFs and was attributed to the narrow channels in the framework and the strong interactions of H_2 under the localized charge densities.[19] Following the experiment, a simulation study was reported to examine H_2 adsorption in *soc*-MOF. The isosteric heats were predicted to be 14.354 and 10.645 kJ/mol at unsaturated and saturated states, respectively.[20] These values are substantially higher than the experimentally measured 6.5 kJ/mol.

A better understanding of the fundamental mechanism for high H_2 adsorption in charged *soc*-MOF is of importance, which could facilitate the development of new MOFs for further enhanced H_2 storage. In this work, we first investigate, using atomistic simulations, the distribution and dynamics of the extraframework NO_3^- ions in *soc*-MOF. The microscopic properties of extraframework ions in nanoporous materials are crucial to elucidating and tailoring their functionality, and subsequently to improve storage, catalytic, ion exchange, and conductivity. We then simulate the isotherm and isosteric heat of H_2 adsorption and identity the favorable adsorption sites. As we shall see, fairly good agreement is obtained with experimental measurements. In addition, syngas purification is considered in *soc*-MOF. The syngas is initially mimicked as a two-component mixture of H_2 and CO_2, then as a four-component mixture of H_2, CO_2, CO, and CH_4, and finally as a five-component mixture including a trace of H_2O to examine the effect of H_2O on separation. The as-synthesized *soc*-MOF is insoluble in H_2O and common organic solvents. It is worthwile to note that exceptionally high selective adsorption for CO_2/CH_4 mixture in *soc*-MOF was found in our recent work, to the best of our knowledge, which represents the first study examining gas mixture in a charged MOF.[21]

The models for *soc*-MOF framework, NO_3^- ion, and adsorbates (CO_2, H_2, CO, CH_4, and H_2O) are described in Models section, followed by methodology in Methodology section. Specifically, canonical Monte Carlo (MC) and molecular dynamics (MD) simulations were used to examine the distribution and dynamics of NO_3^- ions in *soc*-MOF. Gibbs ensemble MC (GEMC) and grand canonical MC (GCMC) simulations were used to predict the adsorption of H_2 and mixtures, respectively. The adsorption isotherm, isosteric heat, simulation snapshot, and selectivity are presented and discussed in Results and Discussion section. Finally, the concluding remarks are summarized in Conclusions section.

Models

The charged *soc*-MOF has a molecular formula $[In_3O(C_4N_{0.5}O_2H_{1.5})_6](NO_3)$. It consists of rare *soc* topology assembled by oxygen-centered indium-carboxylate trimer $[In_3O(CO_2)_6]$ building blocks. Each trimer contains three octahedra that are joined with six azobenzene organic linkers. There exist carcerand-like capsules and infinite narrow channels (~1 nm in diameter). A capsule is isolated by eight trimers connecting with six linkers and surrounded by narrow channels. The indium atoms in *soc*-MOF are trivalent, yielding a cationic framework that is charge balanced by NO_3^- ions. As shown in Figure 1, a unit cell of *soc*-MOF contains eight NO_3^- ions, in which four NO_3^- ions are located tetrahedrally in the central capsule with N—N distance of 9.3 Å and the other four NO_3^- ions are located in different capsules of the periodic cells. In our recent study,

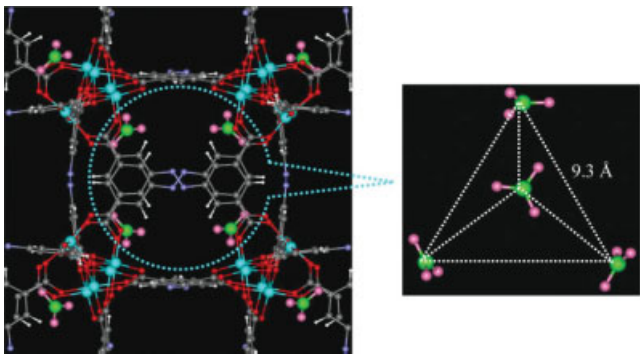

Figure 1. A unit cell of *soc*-MOF with eight charge balancing extraframework NO_3^- ions.

Four NO_3^- ions are located tetrahedrally in the central carcerand-like capsule and the other four are located in different capsules. [Color figure can be viewed in the online issue, which is available at www.interscience.wiley.com.]

NO_3^- ions were simply assumed being distributed freely in *soc*-MOF and their locations were identified by simulation.[21] The experimental study for H_2 adsorption in *soc*-MOF was conducted in dehydrated form;[19] consequently, in this work, we consider the dehydrated *soc*-MOF (removing ligand H_2O molecules from the capsules and channels and from the apical positions of trimer building blocks).

The atomic charges of *soc*-MOF framework atoms were calculated from density-functional theory (DFT) based on the fragmental cluster illustrated in Figure 2. The Lee–Yang–Parr correlation functional (B3LYP) was used in the DFT calculation with Gaussian 03 package. To maintain the correct hybridization, the dangling C—C bonds in the cluster were terminated by CH_3 group. It has been commonly recognized that quantum mechanically derived charges fluctuate appreciably when small basis set is used. Nevertheless, they tend to converge beyond the basis set 6-31G(d).[22] Therefore, 6-31G(d) basis set was used in the DFT calculations for all

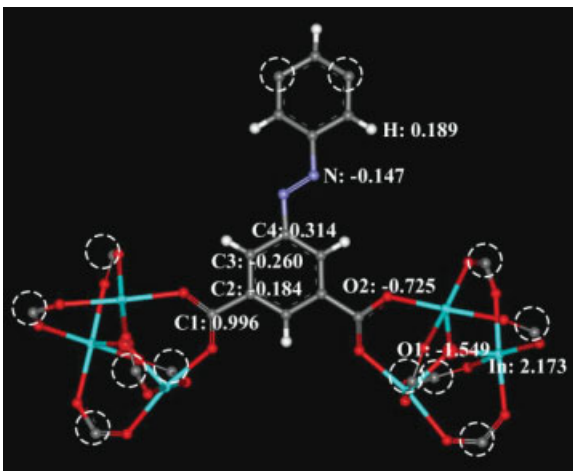

Figure 2. Atomic charges of *soc*-MOF framework calculated from density-functional theory.

To maintain the correct hybridization, the dangling C—C bonds (indicated by the dashed circles) in the fragmental cluster were terminated by —CH_3 groups. [Color figure can be viewed in the online issue, which is available at www.interscience.wiley.com.]

atoms except the indium atoms, for which LANL2DZ basis set was used. LANL2DZ is a double-zeta basis set and contains effective pseudo-potentials to represent the potentials of nucleus and core electrons experienced by the valence electrons. This allows only the softer valence electron wave-functions, which usually control the chemistry, to be explicitly treated and can significantly reduce computational cost. After the DFT calculation, the atomic charges were estimated by fitting to the electrostatic potentials. The dispersion interactions of the framework atoms were presented by Lennard-Jones (LJ) potential with parameters from the universal force field (UFF).[23] The Lorentz-Berthelot combining rules were used to calculate the cross interaction parameters. A number of simulation studies have shown that UFF can accurately predict the adsorption and diffusion of gases in various MOFs.[24–29] For instance, good agreement was obtained for Ar adsorption in Cu-BTC between simulation and experiment.[24] Simulated adsorption isotherms and diffusivities of CO_2 and CH_4 in IRMOF-1 match well with experimental data.[27–29]

The extraframework NO_3^- ion in *soc*-MOF was considered as being rigid with a bond length N—O of 1.302 Å and a bond angle ∠ONO of 120°. The atomic charges of NO_3^- ions were adopted from ab initio calculations with $0.197e$ for N atom and $0.399e$ for O atom.[30] H_2 was mimicked as a two-site model with the LJ potential parameters fitted to the isosteric heat of H_2 adsorption on a graphite surface.[7] CO_2 was represented as a three-site rigid molecule and its intrinsic quadrupole moment was described by a partial charge model.[31] The partial charges on C and O atoms were $q_C = 0.576e$ and $q_O = -0.288e$ ($e = 1.6022 \times 10^{-19}$), respectively. The C—O bond length was 1.18 Å and the bond angle ∠OCO was 180°. CH_4 was represented by a united-atom model with the LJ potential parameters from the TraPPE force field that was developed to reproduce the critical parameters and saturated liquid densities of alkanes.[32] CO was modeled as two-site with the LJ potential parameters fitted to the heat of CO adsorption on exfoliated graphite (grafoil).[33] To examine the effect of H_2O on syngas separation, H_2O was included in a five-component mixture with H_2O represented by TIP3P (three-point transferable interaction potential) model.[34] Table 1 gives the force field parameters of the extraframework ion and adsorbates.

Methodology

To examine the locations and dynamics of NO_3^- ions, canonical MC simulation was performed at 298 K. The

Table 1. Force Field Parameters of Extraframework Ion and Adsorbates

Species	Site	σ(Å)	ε/k_B(K)	q (e)
NO_3^-	N	3.260	34.690	+0.197
	O	3.118	30.166	−0.399
H_2	H	2.59	12.5	0
CO_2	C	2.789	29.66	+0.576
	O	3.011	82.96	−0.288
CO	C	3.385	39.89	0
	O	2.885	61.57	0
CH_4	CH_4	3.73	148.0	0
H_2O	OW	3.151	76.42	−0.834
	HW	–	–	+0.417

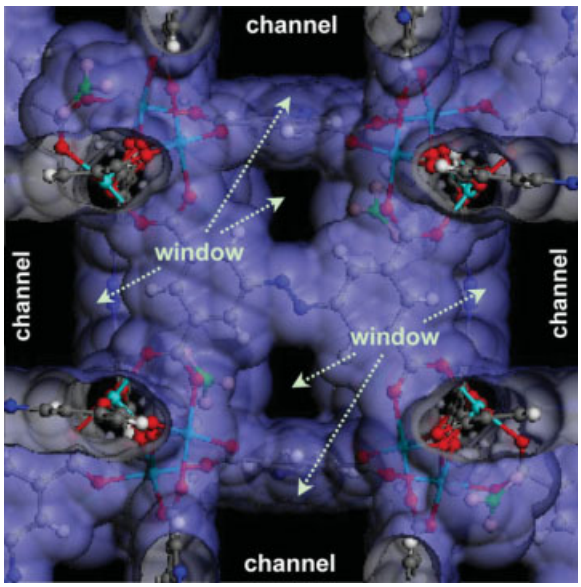

Figure 3. Channels and windows in a unit cell of *soc*-MOF.

The central capsule is accessible from the surrounding channels through the restricted windows. [Color figure can be viewed in the online issue, which is available at www.interscience.wiley.com.]

simulation box contained a unit cell of *soc*-MOF with eight NO_3^- ions and the periodic boundary conditions were applied. The initial positions of NO_3^- ions, as shown in Figure 1, were adopted from experimental crystallographic data. The framework was assumed as being rigid and the framework atoms were fixed during simulation. As a consequence, the unit cell was divided into three-dimensional grids with the potential energy tabulated in advance and then used by interpolation during simulation. Such a treatment accelerated the simulation by approximately two orders of magnitude. A spherical cutoff of 11.2 Å was used to evaluate the LJ interactions. Beyond the cutoff, the usual long-range corrections for homogeneous system were used.[35] The use of the usual long-range corrections was an appropriate approximation because the error introduced by assuming homogeneity was small compared with the magnitude of the long-range corrections.[36] For the Coulombic interactions, a simple spherical truncation could result in significant errors; consequently, Ewald sum with a tin-foil boundary condition was used instead.[37] The real/reciprocal space partition parameter and the cutoff for reciprocal lattice vectors were chosen to be 0.2 $Å^{-1}$ and 8, respectively, to ensure the convergence of Ewald sum. These methods to evaluate the LJ and Coulombic interactions were also used in the simulations for the adsorption of H_2 and syngas, respectively. A total of 10^7 trial moves were carried out to sample the configurational space of NO_3^- ions. Two types of trial moves, translation and rotation, were used with equal probability. To quantitatively characterize the dynamics of NO_3^- ions, MD simulation was performed using DL_POLY program.[38] The starting configuration for MD was generated directly from the MC simulation mentioned earlier. The Nosé-Hoover thermostat was used to maintain a constant temperature of 298 K. The MD simulation was performed for 3 ns, including 1 ns equilibration and 2 ns production. The potential and kinetic energies were monitored during the MD simulation to ensure equilibration. The time step was 1 fs for good energy conservation and history file was saved every 1 ps for analysis.

Most extant simulation studies for adsorption use GCMC method at fixed chemical potential, volume, and temperature. The chemical potential as an input in GCMC has to be converted into pressure upon comparison with experiment. This has to be implemented using empirical equations of state or additional simulations. For H_2 adsorption under this study, we used GEMC simulation directly at a desired pressure. To do this, two simulation boxes were used one for *soc*-MOF adsorbent and the other for bulk H_2. The total number of H_2 molecules was fixed, but they could swap from one box to the other. The volume of *soc*-MOF was fixed, whereas the volume of bulk phase fluctuated at fixed bulk pressure. During adsorption, the locations of NO_3^- ions were not fixed and could move by translation and rotation. Four types of trial moves were conducted for H_2 molecules including translation and rotation in each phase, swap between the two phases, and volume change of the bulk phase. It should be noted that H_2 molecules were not allowed to insert randomly into the capsules during swap move, but they might move into there by translation from the surrounding channels. This is to mimic experimental observation that the isolated cuboidal capsules are strictly accessible from the channels via restricted windows.[19] Figure 3 shows the channels surrounding the central capsule, along with the restricted windows as entrance. The isolated capsule is accessible solely via the windows (7.651 Å × 5.946 Å in dimensions). The total number of trial moves in a typical simulation was 2×10^7, with the first 10^7 moves used for equilibration and the second 10^7 moves to obtain ensemble averages. The block transformation method was used to estimate the statistical uncertainties of simulated averages.[37] Unless otherwise mentioned, the uncertainties were smaller than the symbol sizes in the figures presented.

In our previous studies, GEMC has been used successfully to simulate the adsorption of O_2 and N_2 in carbon-based materials,[39,40] CH_4 and H_2O in ETS-10,[41] and CO_2 in MOFs[28] and COFs.[42] The beauty of GEMC simulation is that one can obtain uptake directly at a desired bulk pressure, as well as the bulk density and enthalpy that are required to calculate excess adsorption and isosteric heat. To precisely characterize adsorption mechanism, isosteric heat rather than adsorption isotherm is usually used, as the former is more sensitive to the change of adsorption energy. In our work, the isosteric heat q_{st} was calculated from

$$q_{st} = H_b - \left(\frac{\partial U_a}{\partial N_a}\right)_{T,V}, \quad (1)$$

where H_b is the enthalpy of adsorbate in bulk phase obtained from GEMC simulation. In most GCMC simulation studies, H_b is simply assumed to be RT in which R is gas constant. This assumption is acceptable when the bulk phase behaves as an ideal gas, but not accurate at high pressure and/or low temperature. U_a is the total adsorption energy including contributions from adsorbate–adsorbent and adsorbate–adsorbate interactions, and N_a is the number of adsorbed molecules.

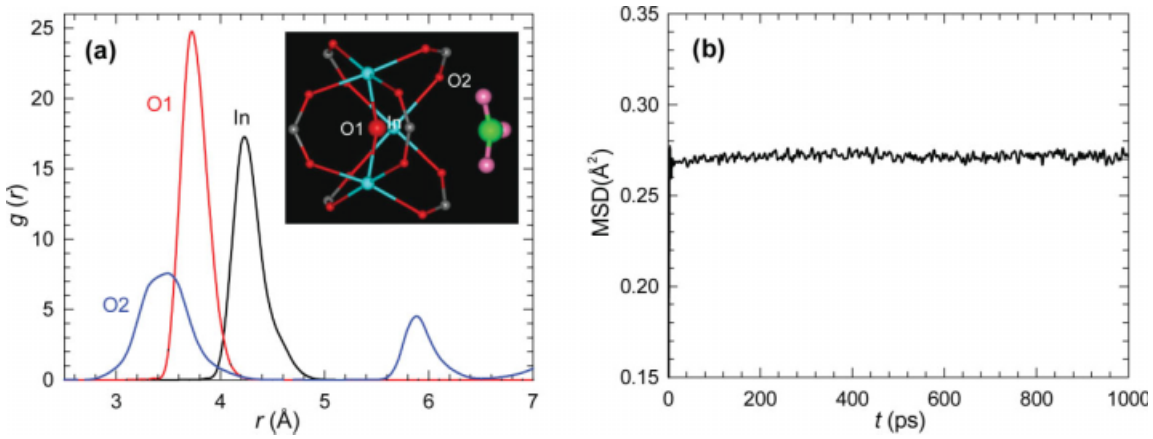

Figure 4. (a) Radial distribution functions of NO_3^- ions around In, O1, and O2 atoms of trimer $[In_3O(CO_2)_6]$. The inset illustrates the location of NO_3^- ion near trimer. (b) Mean-squared displacement of NO_3^- ions.

[Color figure can be viewed in the online issue, which is available at www.interscience.wiley.com.]

There are two ways to evaluate the derivative in Eq. 1, by direct differentiation or fluctuation theory; the former was used here.

GEMC is not readily applicable to simulate the adsorption of mixture with a fixed composition. Consequently, GCMC simulations were used for the adsorption of syngas. The syngas was mimicked, progressively more complicated, as two-, four-, or five-component mixtures. The bulk compositions were $CO_2/H_2 = 15:85$ for two-component mixture and $CO_2/H_2/CO/CH_4 = 15:75:5:5$ for four-component mixture. To examine the effect of trace amount of H_2O, 0.1% of H_2O was added into the four-component mixture. The total number of trial moves in the GCMC was 2×10^8. Six types of trial moves were randomly attempted, namely, translation, rotation, and partial regrowth at a neighboring position; complete regrowth at a new position; swap with the reservoir including creation and deletion with equal probability; and identity exchange of molecules. Similar to H_2 adsorption in GEMC simulation, the adsorbate molecules were not allowed to insert into the capsules during regrowth and creation moves. Although identity exchange is usually not required in GCMC simulation, its use allows faster equilibration and reduces fluctuation after equilibration. NO_3^- ions were allowed to move by translation and rotation in the simulations.

Results and Discussion

We first present the static and dynamic properties of extraframework NO_3^- ions, including locations, radial distribution functions, and temporal mean-squared displacement (MSD). Then, the adsorption properties of H_2 at 78 K are shown. Favorable binding sites are identified with increasing pressure; adsorption isotherm and isosteric heat are compared with experimental data. Finally, the adsorption and separation of syngas at 298 K are investigated for two-, four-, and five-component mixtures. The locations of H_2O in *soc*-MOF and the effect of H_2O on separation are examined.

Locations and dynamics of NO_3^- ions

Eight NO_3^- ions exist in a unit cell of *soc*-MOF and have similar crystalline environment. The final locations of NO_3^- ions from MC simulation are close to the initial positions in Figure 1, which implies that NO_3^- ions cannot escape from the capsule because of steric hindrance. As illustrated by Figure 3, the capsule is accessible from the surrounding channels via restricted windows; consequently, the energy barrier for NO_3^- ions to come across is high. In the capsule, there exist eight corners proximal to the corner-sharing octahedral trimers. Each NO_3^- ion occupies statistically two corners with equal probability. This is in good accordance with experimental observation.[19] To quantitatively identify the locations, the radial distribution functions of NO_3^- ions around trimer $[In_3O(CO_2)_6]$ were calculated from

$$g_{ij}(r) = \frac{\Delta N(r, r+\Delta r)V}{4\pi r^2 \Delta r N_i N_j} \tag{2}$$

where r is the distance from the center-of-mass of NO_3^- (i.e., the N atom) to an atom of trimer, $\Delta N(r,r+\Delta r)$ is the coordination number within a shell from r to $r+\Delta r$, V is the system volume, $N_i(N_j)$ is the number of species i (j). Figure 4a shows the radial distribution functions of NO_3^- ions around In, O1, and O2 atoms of trimer. The inset illustrates the typical location of NO_3^- ion near trimer. A trimer contains three In atoms, one central O1 atom and 12 carboxyl O2 atoms. NO_3^- ion has an equal probability to the three In atoms with a distance of 4.3 Å. From NO_3^- ion to O1 atom, the distance is 3.7 Å; and from NO_3^- to O2 atom, the distance is 3.4 Å. Apparently, NO_3^- ion is closer to O2 atom than O1 atom. However, the first peak of $g(r)$ around O2 is lower than that around O1. This is simply because there are 12 O2 atoms and coordination number was divided by 12 to calculate the relative density using Eq. 2. The existence of second peak of $g(r)$ around O2 is because of the O2 atoms on the other side of trimer. The extraframework NO_3^- ions in *soc*-MOF behave differently from the extraframework Na^+ ions in titanosilicate ETS-10. In a recent study, five types of Na^+ ions were identified to exist in ETS-10 with various coordination environments and site energies; type-V Na^+ ions exhibit substantially greater mobility than other types.[41]

The dynamics of extraframework ions was characterized by the MSD from MD simulation

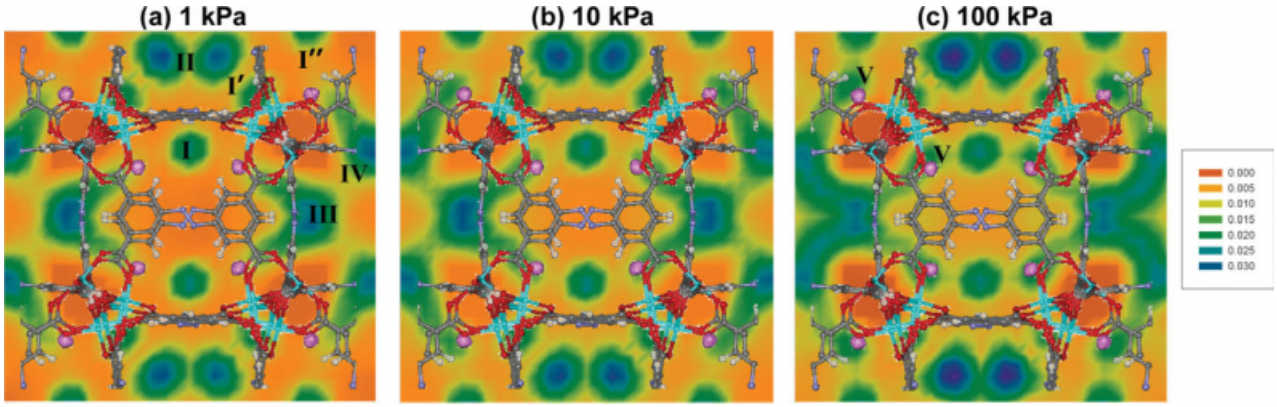

Figure 5. Density contours of H_2 molecules for the adsorption of H_2 at 1, 10, and 100 kPa, respectively.

Temperature $T = 78$ K. The center-of-mass distributions of NO_3^- ions are denoted by purple balls. [Color figure can be viewed in the online issue, which is available at www.interscience.wiley.com.]

$$\mathrm{MSD}(t) = \left\langle \frac{1}{N}\sum_{i=1}^{N} \left|\mathbf{r}_i(t) - \mathbf{r}_i(0)\right|^2 \right\rangle, \tag{3}$$

where t is time, N is the number of NO_3^- ions, and $\mathbf{r}_i(t)$ is the center-of-mass position of ion i at time t. The multiple time-origin method was used for better statistical accuracy. Figure 4b demonstrates that the MSD of NO_3^- ions is very small and fluctuates marginally around 0.27 Å^2. Consistent with the finding from MC simulation discussed earlier, the negligible mobility reveals that NO_3^- ions essentially vibrate in the capsule. This is attributed to the tight binding of NO_3^- ions with trimers and the steric restriction of capsule. The movie of NO_3^- ions is provided in the Supporting Information.

H_2 adsorption

To identify the favorable adsorption sites of H_2 adsorption at 78 K, Figure 5 shows the density contours of H_2 molecules at 1, 10, and 100 kPa from GEMC simulations. At different pressures, the center-of-mass distributions of NO_3^- ions are nearly identical in the capsules, implying that the locations of NO_3^- ions are not influenced discernibly by H_2 adsorption. At low pressure (1 kPa), H_2 is adsorbed preferentially at four different types of sites. Site I is between two exposed indium atoms (4–5 Å to In atoms) along the x direction and at the entrance of capsule. Site I′ or I″ has the similar geometry but is along the z or y direction. These sites are symmetrical in the crystalline structure and small in size. Consequently, they can accommodate only a few molecules and get saturated rapidly at low pressure. Site II is on the top of azobenzene and parallel to azo backbone (—N=N—). Site III is near azobenzene and perpendicular to azo backbone, also at the entrance of capsule. Site IV is on the top of phenyl moiety and proximal to carboxylate group. The adsorption at the favorable sites identified from simulation is in good agreement with experiment, in which the concurrent occupation of multiple sites was found at low loading. From inelastic neutron scattering (INS), Liu et al. observed a well-defined peak at 25.5 meV due to adsorption at the exposed indium sites and other two peaks at 12.8 and 14.0 meV associated with the organic components.[19] The presence of multiple adsorption sites in *soc*-MOF leads to a homogeneous distribution of adsorption energy landscape; as a consequence, the isosteric heat of adsorption is relatively a constant as discussed later. At moderate pressure (10 kPa), site I is already saturated and more H_2 molecules are adsorbed at sites II, III, and IV. This is consistent with the INS measurement that there was a pronounced increase in intensity with loading at 12.8 and 14.0 meV, but not at 25.5 meV. At high pressure (100 kPa), all the adsorption sites I–VI are almost fully occupied and site II appears to possess the largest density. Compared to the case at 10 kPa, more molecules are adsorbed in the region between sites III and IV. Intriguingly, adsorption at 100 kPa also occurs at a new site V in the capsule. This is supported remarkably by INS spectra in experiment.[19] As illustrated in Figure 3, the capsule in *soc*-MOF is isolated and accessible only through the surrounding infinite channels by restricted windows. As a result of the high energy barrier to come across the entrance, the capsule is not accessible to H_2 at low pressure. Driven by high pressure (external force), however, H_2 molecules can enter into the capsule at 100 kPa. There are eight corners proximal to eight trimers in the capsule, in which four of them are occupied by tetrahedrally located NO_3^- ions and the other four by H_2 molecules.

Figure 6a shows the isotherm of H_2 adsorption in *soc*-MOF at 78 K. The simulated uptake agrees fairly well with experiment,[19] though slight underestimation at low pressure and overestimation at pressure over 1 bar. The deviations from experiment data could be attributed primarily to two factors. First, the *soc*-MOF in our simulation is a perfect crystal, whereas experimental sample may contain impurities. The impurities are dispersed in the channels and lead to a stronger interaction with adsorbate, consequently, enhance adsorption at low pressure. On the other hand, the impurities block the channels and decrease free volume, then reduce adsorption capacity at high pressure. Second, the force field used in the simulation may not be very accurate and needs to be improved, for example, to include polarization effect. The adsorbate molecules are under the electric field of charged framework and extraframework ions, therefore, polarization might occur. As found experimentally and also in our simulation, H_2 uptake in *soc*-MOF at 78 K and 1

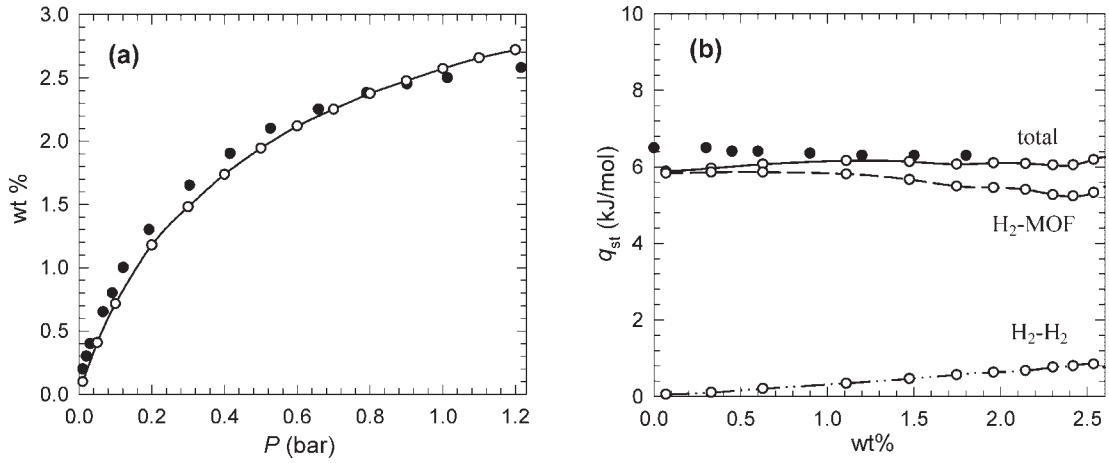

Figure 6. H_2 adsorption at 78 K (a) isotherm and (b) isosteric heat.

Simulation results: open symbols; experimental data: filled symbols.[19] The isosteric heat from simulation is decomposed into two contributions, H_2-MOF and H_2–H_2.

atm approaches a liquid-like state of H_2 (0.0708 g/cm^3 at boiling point of 20 K and 1 atm) and is substantially higher than in IRMOF-1[43] and most MOFs reported to date.[44] The high uptake is driven by the nanometer channels, the localized charges in framework, and the exposed metal sites. The nanometer channels have narrow diameter, leading to a strong overlap of potential energy fields, particularly, near the trimers.

Figure 6b shows the isosteric heat q_{st} of H_2 adsorption in *soc*-MOF at 78 K. The simulated q_{st} matches well with experimental data, particularly, at intermediate and high loadings.[19] The magnitude of q_{st} is comparable to H_2 adsorption in other ion-exchanged MOFs and zeolites.[45–48] At infinite dilution, q_{st} is about 6.0 kJ/mol from simulation, slightly lower than 6.5 kJ/mol by experiment. The Henry's constant is 0.38 mmol kPa^{-1} cm^{-3} from simulation. With increased loading, q_{st} remains nearly a constant. To further examine its behavior, q_{st} was decomposed into two contributions, one from H_2–H_2 interaction and the other from H_2-MOF interaction. The contribution from H_2–H_2 interaction rises as loading increases because of the increasingly greater cooperative attraction between adsorbed H_2 molecules. In contrast, the contribution from H_2-MOF interaction drops with loading. This is because adsorption first occurs at the most favorable sites and then in less favorable sites; consequently, H_2-MOF interaction becomes weaker when more H_2 is adsorbed. Nevertheless, the drop in H_2-MOF interaction is insignificant, which reveals the relatively homogenous characteristics of adsorption sites in *soc*-MOF framework. This type of behavior was also observed for SF_6 adsorption in alumina.[49]

Syngas purification

Adsorption of two-component mixture CO_2/H_2 with a bulk composition of 15:85 was simulated in *soc*-MOF at 298 K. As seen in Figure 7a, CO_2 is far more adsorbed than H_2 because of three reasons. First, CO_2 is a three-site molecule and has a much stronger interaction with the framework than H_2. Second, the temperature 298 K considered is subcritical for CO_2 (T_c = 304.4 K), but supercritical for H_2 (T_c = 33.2 K); that is, CO_2 is substantially more condensable than H_2 at 298 K. It was observed in many studies that H_2 adsorption at room temperature is quite small in various MOFs, though the adsorption could be rather high at cryogenic temperatures.[11,50] Third, the highly ionic framework and presence of

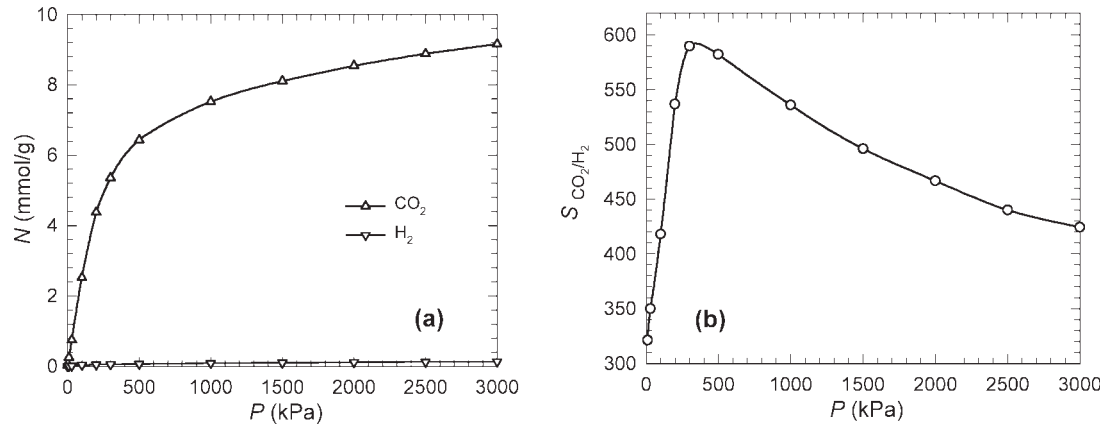

Figure 7. Adsorption of two-component mixture CO_2/H_2 (15:85) at 298 K.

(a) isotherm and (b) selectivity of CO_2 over H_2.

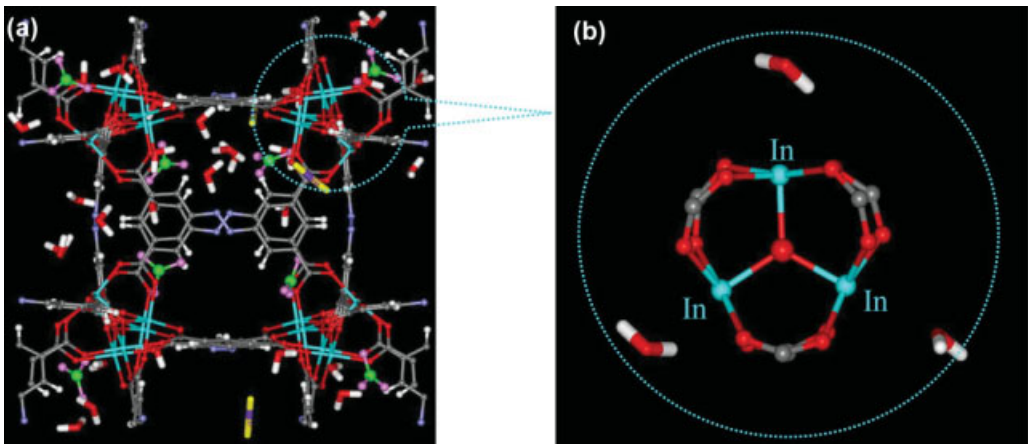

Figure 8. (a) Snapshot for the adsorption of five-component mixture $CO_2/H_2/CO/CH_4/H_2O$ (15:75:5:5:0.1) at 10 kPa and 298 K. (b) Locations of H_2O molecules around $[In_3O(CO_2)_6]$.

Color code: In, cyan; O, red; C, gray; N, blue; H, white; NO_3^-, green for N and pink for O; CO_2 and H_2O are shown in stick mode. [Color figure can be viewed in the online issue, which is available at www.interscience.wiley.com.]

extra framework NO_3^- ions induce strong electrostatic interactions with quadrupolar CO_2 molecules, and thus enhance the adsorption for CO_2. The separation factor of CO_2/H_2 mixture is quantified by adsorption selectivity defined by

$$S_{i/j} = (x_i/x_j)(y_j/y_i), \tag{4}$$

where x_i and y_i are the mole fractions of component i in adsorbed and bulk phases, respectively. Figure 7b shows the selectivity of CO_2 over H_2 as a function of total pressure. With increasing pressure, the selectivity increases sharply, passes a maximum of about 600 at 300 kPa, and then decreases. It can be expected that the selectivity will reach a plateau upon further increasing pressure. The initial increase at low pressure is caused by the strong interactions between CO_2 molecules and multiple binding sites in *soc*-MOF, and further promoted by the cooperative interactions of adsorbed CO_2 molecules. The decrease in selectivity is attributed primarily to the entropy (packing) effect at high pressure. H_2 molecules are smaller in size and can fit into the channels more effectively, leading to a decrease in selectivity.

We further simulated the adsorption of four-component mixture ($CO_2/H_2/CO/CH_4$ = 15:75:5:5) and five-component mixture ($CO_2/H_2/CO/CH_4/H_2O$ = 15:75:5:5:0.1) in *soc*-MOF to mimic a typical syngas without and with the presence of H_2O. In some adsorption processes, the presence of H_2O is adverse, for example, a very small amount of H_2O in Li-LSX zeolite significantly affects the adsorption capacity of atmospheric gases, such as N_2, O_2, and Ar, because of the shielding of cation sites by H_2O.[51] Similarly, the adsorption capacity of CO_2 on several different cationic forms of zeolite X is inhibited by the presence of H_2O.[52] In some cases, however, a small amount of H_2O can be beneficial, for example, the presence of preadsorbed H_2O in the supercages of BaX zeolite increases the selectivity toward *p*-xylene in an equimolar *p*-xylene/*m*-xylene mixture.[53] A recent study revealed a pronounced increase in selectivity of CO_2 over CH_4 in a hydrated form of MIL-53 compared with a dehydrated form.[54]

Similar to the two-component mixture CO_2/H_2, CO_2 is more strongly adsorbed than other simple gases (H_2, CO, and CH_4) in the four- or five-component mixture over the entire range of pressure. Nevertheless, the presence of a tiny amount of H_2O has a significant influence. Figure 8a shows the simulation snapshot of five-component mixture at 10 kPa and 298 K. The adsorption of CO, CH_4, and H_2 is negligible; therefore, they are not observed in the snapshot. Despite the large molar ratio of CO_2 over H_2O (15/0.1 = 150), H_2O is predominantly adsorbed against CO_2. Unlike other simple gases present in the mixture, H_2O is a highly polar molecule and strongly bound to the exposed indium atoms of trimer $[In_3O(CO_2)_6]$. As shown in Figure 8b, a trimer is surrounded by three H_2O molecules and the distance from the O atom of H_2O to the indium atom of trimer is ~3.2–3.4 Å. In a recent simulation study on H_2O adsorption in Cu-BTC, it was also found that H_2O is strongly coordinated to metal atoms.[55]

Figure 9 shows the density contours of CO_2 and H_2O molecules for the adsorption of five-component mixture ($CO_2/H_2/CO/CH_4/H_2O$= 15:75:5:5:0.1) at 10, 100, and 1000 kPa, respectively. As the adsorption of CO, CH_4, and H_2 from the mixture is vanishingly small, their density contours were not plotted. Similar to Figure 5a for H_2 adsorption at 78 K, at 10 kPa CO_2 is preferentially adsorbed at sites I–IV. Nevertheless, the temperature here is 298 K, which results in a high thermal motion of adsorbate molecules, the locations of CO_2 are more dispersed compared to Figure 5a. The region near trimer is also occupied by small amount of CO_2, which is not observed in Figure 5a. This is induced by H_2O molecules adsorbed surrounding trimer. As illustrated in Figure 8b, the positively charged exposed indium atoms of trimer strongly interact with H_2O and the bound H_2O molecules act as additional sites for CO_2 near trimer. With increasing pressure from 10 to 100 and 1000 kPa, CO_2 at site I is completely replaced by H_2O and more CO_2 is adsorbed at sites II–IV; the density of H_2O increases around trimer and additionally H_2O enters the capsule occupying site V, but CO_2 cannot enter. This is due to the fact that H_2O has a

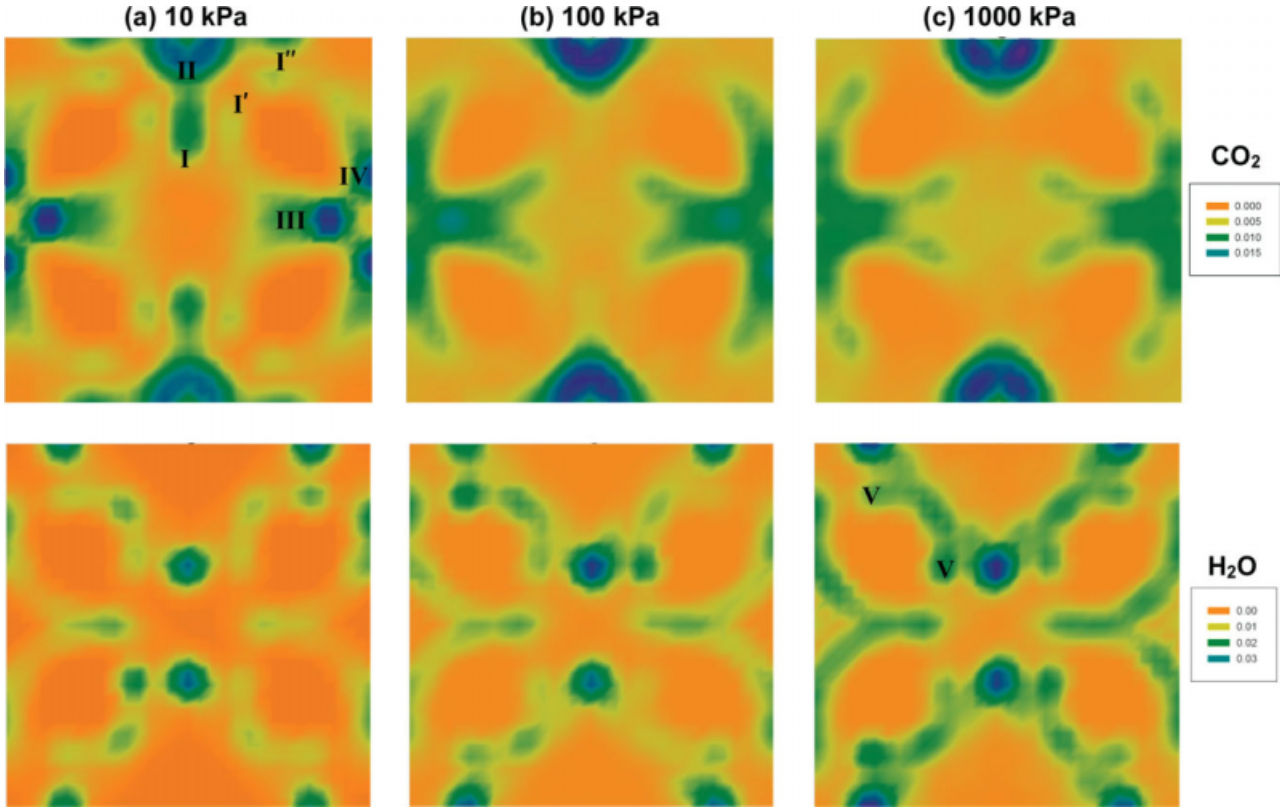

Figure 9. Density contours of CO_2 and H_2O molecules for the adsorption of five-component mixture $CO_2/H_2/CO/CH_4/H_2O$ mixture (15:75:5:5:0.1) at 10, 100, and 1000 kPa, respectively.

Temperature $T = 298$ K. For clarity, the framework and extraframework ions are not shown. [Color figure can be viewed in the online issue, which is available at www.interscience.wiley.com.]

significantly stronger interaction than CO_2 with the NO_3^- ions in the capsule. The simulation results interestingly reveal a promoted adsorption of CO_2 by H_2O at low pressure and a competitive adsorption between them at high pressure.

Figure 10 shows the adsorption selectivity of CO_2/H_2 in two-, four-, and five-component mixtures from simulation. As a function of total pressure, similar trend is found in all the three mixtures; that is, the selectivity increases up to a maximum and then decreases. Compared to two-component mixture, the selectivity in four-component mixture slightly decreases. As mentioned, CO and CH_4 interact weakly with *soc*-MOF and their adsorption is negligible. Therefore, their presence only leads to a small change in selectivity. Nevertheless, in the presence of even a trace of H_2O in five-component mixture, H_2O largely affects the selectivity. At low pressure, the selectivity slightly rises because of the promoted adsorption of CO_2 by H_2O that act as additional sites. In marked contrast, competitive adsorption occurs at high pressure and H_2O substitutes preadsorbed CO_2; consequently, the selectivity of CO_2/H_2 drops.

The selectivity of CO_2/H_2 in two-component mixtures is close to 600 at 300 kPa, which is the typical operating pressure for pressure-swing adsorption. In the presence of H_2O, the maximum selectivity drops to 550. The adsorption and selectivity of CO_2/H_2 mixtures have also been studied in other nanoporous materials by experiments or simulations. For example, the selectivity is ~5 in silicalite and 3.5 in ETS-10 for an equimolar CO_2/H_2 mixture.[13] In an activated carbon, the selectivity ranges from 60 to 90 for different mole fractions of CO_2/H_2 mixtures.[14] The selectivity is ~70 in zeolite Na-4A for a mixture with composition of 98.6% H_2

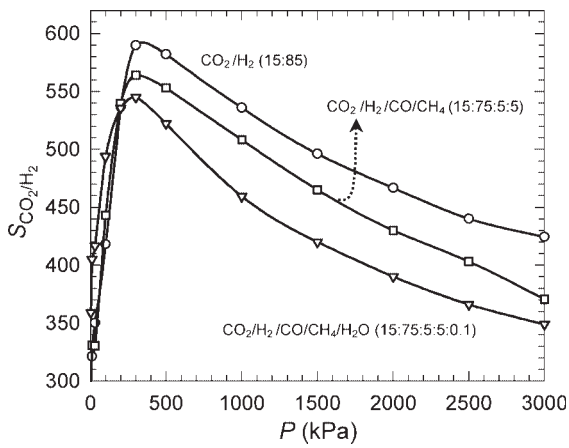

Figure 10. Selectivity of CO_2 over H_2 in two-, four-, and five-component mixtures.

The compositions are in the parentheses.

and 1.4% CO_2.[16] The selectivity is ~150 in Cu-BTC and 40 in IRMOF-1 for various compositions of CO_2/H_2 mixtures at 298 K and 0.1 MPa.[17] The selectivity of CO_2/H_2 in *soc*-MOF from this study is the highest in MOFs and significantly higher than other nanoporous materials reported in the literature. In our recent study, we also found the highest selectivity of CO_2 over CH_4 in *soc*-MOF compared to other MOFs.[21] These reveal that the charged *soc*-MOF might be very useful for the separation of CO_2 from syngas, biogas, or natural gas.

Conclusions

The static and dynamic properties of extraframework NO_3^- ions, H_2 adsorption, and syngas purification in charged *soc*-MOF were investigated using atomistic simulations. A clear understanding in the microscopic properties of extraframework ions is critical to tailoring the functionality of nanoporous materials. NO_3^- ions were found to reside in the carcer-and-like capsules and cannot escape because of restricted windows. In a capsule, four NO_3^- ions are distributed statistically near eight trimer building blocks with equal probability. The mobility of NO_3^- ions is negligible attributed to the strong interactions with highly ionic framework and the steric hindrance.

The simulated isotherm and isosteric heat of H_2 adsorption in *soc*-MOF at 78 K agree fairly well with experimental data. The extent of adsorption in *soc*-MOF is substantially larger than in most reported MOFs. This is a consequence of the strong interactions between H_2 and the narrow nanometer-scale channels, the localized charges, and the exposed metal sites. The isosteric heat is about 6.0 kJ/mol at infinite dilution and changes slightly as loading increases. The weak loading dependence of isosteric heat suggests that adsorption sites in *soc*-MOF are relatively homogenously distributed. This is consistent with the concurrent occupation of multiple adsorption sites. H_2 adsorbs at sites I–IV at low pressure and also at site V at high pressure. Interestingly, site V is in the capsule and only accessible at high pressure through the surrounding channels via restricted windows. These simulated results are supported remarkably by experimental observations.

For syngas purification, two-, four-, and five-component mixtures were considered with increasing complexity. In two- (CO_2/H_2 = 15:85) and four-component ($CO_2/H_2/CO/CH_4$ = 15:75:5:5) mixtures, CO_2 is more preferentially adsorbed over other gases because of the stronger interactions with ionic framework, whereas the adsorption of H_2, CO, and CH_4 is vanishingly small. The selectivity of CO_2/H_2 in two-component mixture reaches a maximum of about 600. With increasing pressure, the selectivity increases and then decreases. The initial increase is caused by the strong interactions of CO_2 molecule with framework and the cooperative interactions between CO_2 molecules. The decrease in selectivity is attributed to the entropy (packing) effect at high pressure. The selectivity in four-component mixture is approximately the same at low pressure but decreases slightly at high pressure. With the presence of 0.1% H_2O in mixture, the selectivity of CO_2/H_2 slightly rises at low pressure because of the facilitated adsorption of CO_2 by bound H_2O around trimer. At high pressure, the selectivity drops because H_2O competitively replaces CO_2. The predicted CO_2/H_2 selectivity in *soc*-MOF is substantially higher than in all other MOFs and nanoporous materials reported in the literature. The maximum selectivity is 600 and achievable at 300 kPa, which is the typical operating condition for pressure-swing adsorption. Combining with our recent study in which *soc*-MOF shows the highest selectivity toward CO_2/CH_4 mixture, *soc*-MOF turns out to be a promising material for the purification of gas mixtures, particularly for the separation of CO_2 from syngas, biogas, or natural gas. In addition, *soc*-MOF exhibits exceptionally high uptake for H_2 adsorption. We hope our simulation studies could trigger further experimental investigations on new MOFs possessing highly ionic frameworks, narrow-sized channels, and large surface areas for high-efficacy adsorption and separation.

Acknowledgments

The author gratefully acknowledges the support from the National University of Singapore (R-279-000-243-123) and the Singapore National Research Foundation on the Competitive Research Programme (R-279-000-261-281).

Literature Cited

1. U.S. Department of Energy. *Hydrogen, Fuel Cells and Infrastructure Technologies Program: Multi-Year Research, Development and Demonstration Plan*. U.S. Department of Energy, Washington, DC 2005.
2. Hufton JR, Mayorga S, Sircar S. Sorption-enhanced reaction process for hydrogen production. *AIChE J*. 1999;45:248–256.
3. Gundiah G, Govindaraj A, Rajalakshmi N, Dhathathreyan KS, Rao CNR. Hydrogen storage in carbon nanotubes and related materials. *J Mater Chem*. 2003;13:209–213.
4. Eddaoudi M, Kim J, Rosi N, Vodak D, Wachter J, O'Keefe M, Yaghi OM. Systematic design of pore size and functionality in isoreticular MOFs and their application in methane storage. *Science*. 2002;295:469–472.
5. Vitillo JG, Ricchiardi G, Spoto G, Zecchina A. Theoretical maximal storage of hydrogen in zeolitic frameworks. *Phys Chem Chem Phys*. 2005;7:3948–3954.
6. Krishna R, van Baten JM. Insights into diffusion of gases in zeolites. *Micro Meso Mater*. 2008;109:91–108.
7. Cracknell RF. Simulation of hydrogen adsorption in carbon nanotubes. *Mol Phys*. 2002;100:2079–2086.
8. Sagara T, Klassen J, Ganz E. Computational study of hydrogen binding by metal-organic framework-5. *J Chem Phys*. 2004;121:12543–12547.
9. Frost H, Düren T, Snurr RQ. Effects of surface area, free volume, and heat of adsorption on hydrogen uptake in metal-organic frameworks. *J Phys Chem B*. 2006;110:9565–9570.
10. Jung DH, Kim D, Lee TB, Choi SB, Yoon JH, Kim J, Choi K, Choi SH. Grand canonical Monte Carlo simulation study on the catenation effect on hydrogen adsorption onto the interpenetrating metal-organic frameworks. *J Phys Chem B*. 2006;110:22987–22990.
11. Ryan P, Broadbelt LJ, Snurr RQ. Is catenation beneficial for hydrogen storage in metal-organic frameworks? *Chem Commun*. 2008;4132–4134.
12. Richard V, Favre E, Tondeur D, Nijmeijer A. Experimental study of hydrogen, carbon dioxide and nitrogen permeation through a microporous silica membrane. *Chem Eng J*. 2001;84:593–598.
13. Gallo M, Nenoff TM, Mitchell MC. Selectivities for binary mixtures of hydrogen/methane and hydrogen/carbon dioxide in silicalite and ETS-10 by Grand Canonical Monte Carlo techniques. *Fluid Phase Equilib*. 2006;247:135–142.
14. Cao DP, Wu JZ. Modeling the selectivity of activated carbons for efficient separation of hydrogen and carbon dioxide. *Carbon*. 2005;43:1364–1370.
15. Weinberger B, Darkrim-Lamari F, Levesque D. Capillary condensation and adsorption of binary mixtures. *J Chem Phys*. 2006;124:234712.

16. Akten ED, Siriwardane R, Sholl DS. Monte Carlo simulation of single- and binary-component adsorption of CO2, N-2, and H-2 in zeolite Na-4A. *Energy Fuels*. 2003;17:977–983.
17. Yang QY, Zhong CL. Molecular simulation of carbon dioxide/methane/hydrogen mixture adsorption in metal-organic frameworks. *J Phys Chem B*. 2006;110:17776–17783.
18. Bonenfant D, Kharoune M, Niquette P, Mimeault M, Hausler R. Advances in principal factors influencing carbon dioxide adsorption on zeolites. *Sci Technol Adv Mater*. 2008;9:013007.
19. Liu YL, Eubank JF, Cairns AJ, Eckert J, Kravtsov VC, Luebke R, Eddaoudi M. Assembly of metal-organic frameworks (MOFs) based on indium-trimer building blocks: a porous MOF with *soc* topology and high hydrogen storage. *Angew Chem Int Ed*. 2007;46:3278–3283.
20. Belof JL, Stern AC, Eddaoudi M, Space B. On the mechanism of hydrogen storage in a metal-organic framework material. *J Am Chem Soc*. 2007;129:15202–15210.
21. Babarao R, Jiang JW, Sandler SI. Molecular simulations for adsorptive separation of CO_2/CH_4 mixture in metal-exposed, catenated and charged metal-organic frameworks. *Langmuir*. 2009;25:5239–5247.
22. Hariharan PC, Pople JA. The effect of d-functions on molecular orbital energies for hydrocarbons. *Chem Phys Lett*. 1972;16:217.
23. Rappe AK, Casewit CJ, Colwell KS, Goddard WA, Skiff WM. UFF, a full periodic table force field for molecular mechanics and molecular dynamics simulations. *J Am Chem Soc*. 1992;114:10024.
24. Vishnyakov A, Ravikovitch PI, Neimark AV, Bulow M, Wang QM. Nanopore structure and sorption properties of Cu-BTC metal-organic framework. *Nano Lett*. 2003;3:713–718.
25. Garberoglio G, Skoulidas AI, Johnson JK. Adsorption of gases in metal organic materials: comparison of simulations and experiments. *J Phys Chem B*. 2005;109:13094–13103.
26. Skoulidas AI, Sholl DS. Self-diffusion and transport diffusion of light gases in metal-organic framework materials assessed using molecular dynamics simulations. *J Phys Chem B*. 2005;109:15760–15768.
27. Babarao R, Hu ZQ, Jiang JW, Chempath S, Sandler SI. Storage and separation of CO_2 and CH_4 in silicalite, C_{168} schwarzite, and IRMOF-1: a comparative study from Monte Carlo simulation. *Langmuir*. 2007;23:659–666.
28. Babarao R, Jiang JW. Molecular screening of metal-organic frameworks for CO_2 storage. *Langmuir*. 2008;24:6270–6278.
29. Babarao R, Jiang JW. Diffusion and separation of CO_2 and CH_4 in silicalite, C_{168} schwarzite,and IRMOF-1: a comparative study from molecular dynamics simulation. *Langmuir*. 2008;24:5474–5484.
30. Lu GW, Li CX, Wang WC, Wang ZH. Structure of KNO_3 electrolyte solutions: a Monte Carlo study. *Fluid Phase Equilib*. 2004;225:1–11.
31. Hirotani A, Mizukami K, Miura R, Takaba H, Miya T, Fahmi A, Stirling A, Kubo M, Miyamoto A. Grand canonical Monte Carlo simulation of the adsorption of CO_2 on silicalite and NaZSM-5. *Appl Surf Sci*. 1997;120:81–84.
32. Martin MG, Siepmann JI. Transferable potentials for phase equilibria. I. United-atom description of *n*-alkanes. *J Phys Chem B*. 1998;102:2569–2577.
33. Piper J, Morrison JA, Peters C. The adsorption of carbon monoxide on graphite. *Mol Phys*. 1984;53:1463–1480.
34. Jorgensen WL, Chandrasekhar J, Madura JD, Impey RW, Klein ML. Comparison of simple potential functions for simulating liquid water. *J Chem Phys*. 1983;79:926–935.
35. Frenkel D, Smit B. *Understanding Molecular Simulations: From Algorithms to Applications*, 2nd ed. San Diego: Academic Press, 2002.
36. Siperstein F, Myers AL, Talu O. Long range corrections for computer simulations of adsorption. *Mol Phys*. 2002;100:2025–2030.
37. Allen MP, Tildesley DJ. *Computer Simulation of Liquids*. Oxford: Oxford University Press, 1987.
38. Smith W, Forester TR. DL_POLY_2.0: a general-purpose parallel molecular dynamics simulation package. *J Mol Graph*. 1996;14:136–141.
39. Jiang JW, Sandler SI. Nitrogen adsorption on carbon nanotube bundles: role of the external surface. *Phys Rev B*. 2003;68:245412.
40. Jiang JW, Sandler SI. Monte Carlo simulation of O_2 and N_2 mixture adsorption in nanoporous carbon (C_{168} Schwarzite). *Langmuir*. 2003;19:5936.
41. Anjaiah N, Zhao XS, Jiang JW. Molecular interplay of cations and nonpolar/polar sorbates in titanosilicate ETS-10. *J Phys Chem C*. 2008;112:12861.
42. Babarao R, Jiang JW. Exceptionally high CO_2 storage in covalent-organic frameworks: atomistic simulation study. *Energy Environ Sci*. 2008;1:139–143.
43. Rowsell JLC, Millward AR, Park KS, Yaghi OM. Hydrogen sorption in functionalized metal-organic frameworks. *J Am Chem Soc*. 2004;126:5666–5667.
44. Collins DJ, Zhou HC. Hydrogen storage in metal-organic frameworks. *J Mater Chem*. 2007;17:3154–3160.
45. Dinca M, Dailly A, Liu Y, Brown CM, Neumann DA, Long JR. Hydrogen storage in a microporous metal-organic framework with exposed Mn^{2+} coordination sites. *J Am Chem Soc*. 2006;128:16876–16883.
46. Georgiev PA, Albinati A, Eckert J. Room temperature isosteric heat of dihydrogen adsorption on Cu(I) cations in zeolite ZSM-5. *Chem Phys Lett*. 2007;449:182–185.
47. Georgiev PA, Albinati A, Mojet BL, Ollivier J, Eckert J. Observation of exceptionally strong binding of molecular hydrogen in a porous material: formation of an eta(2)-H_2 complex in a Cu-exchanged ZSM-5 zeolite. *J Am Chem Soc*. 2007;129:8086–8087.
48. Dinca M, Han WS, Liu Y, Dailly A, Brown CM, Long JR. Observation of Cu^{2+}-H_2 interactions in a fully desolvated sodalite-type metal-organic framework. *Angew Chem Int Ed*. 2007;46:1419–1422.
49. Sircar S. Heat of adsorption on heterogeneous adsorbents. *Appl Surf Sci*. 2005;252:647–653.
50. Kaye SS, Dailly A, Yaghi OM, Long JR. Impact of preparation and handling on the hydrogen storage properties of Zn4O(1,4-benzenedicarboxylate)(3) (MOF-5). *J Am Chem Soc*. 2007;129:14176–14183.
51. Hutson ND, Zajic SC, Yang RT. Influence of residual water on the adsorption of atmospheric gases in Li-X zeolite: experiment and simulation. *Ind Eng Chem Res*. 2000;39:1775–1780.
52. Brandani F, Ruthven DM. The effect of water on the adsorption of CO_2 and C_3H_8 on type X zeolites. *Ind Eng Chem Res*. 2004;43:8339–8344.
53. Moise JC, Bellat JP. Effect of preadsorbed water on the adsorption of *p*-xylene and *m*-xylene mixtures on BaX and BaY zeolites. *J Phys Chem B*. 2005;109:17239–17244.
54. Llewellyn PL, Bourrelly S, Serre C, Filinchuk Y, Ferey G. How hydration drastically improves adsorption selectivity for CO_2 over CH_4 in the flexible chromium terephthalate MIL-53. *Angew Chem Int Ed*. 2006;45:7751–7754.
55. Castillo JM, Vlugt TJH, Calero S. Understanding water adsorption in Cu-BTC metal organic frameworks. *J Phys Chem C*. 2008;112:15934–15939.

Manuscript received Dec. 18, 2008, and revision received Jan. 23, 2009.